Materials Today Bio 32 (2025) 101729

Contents lists available at ScienceDirect

Materials Today Bio

journal homepage: www.journals.elsevier.com/materials-today-bio

Novel anti-pyroptosis drug loaded on metal-organic framework for intervertebral disc degeneration therapy

Yekai Zhang [a,b,c,1], Jiawei Qiu [a,b,c,1], Yiji Chen [c,d,1], Yu Chen [a,b,c,1], Xiaopeng Liu [a,b,c], Hanwen Zhang [a,b,c], Hualin Li [a,b,c], Kaiyu Li [a,b,c], Haobo Ye [a,b,c], Yaosen Wu [a,b,c,*], Xiaolei Zhang [a,b,c,**], Naifeng Tian [a,b,c,***]

[a] Department of Orthopaedics, The Second Affiliated Hospital and Yuying Children's Hospital of Wenzhou Medical University, Wenzhou, 325088, Zhejiang Province, China
[b] The Second School of Medicine, Wenzhou Medical University, Wenzhou, 325035, Zhejiang Province, China
[c] Zhejiang Provincial Key Laboratory of Orthopaedics, Wenzhou, 325035, Zhejiang Province, China
[d] School of Pharmacy, Hangzhou Normal University, Hangzhou, 311121, China

ARTICLE INFO

Keywords:
Intervertebral disc degeneration
Pyroptosis
Pirfenidone
Poly-His6-zinc assembly
PFD@PHZ

ABSTRACT

Intervertebral disc degeneration (IVDD) is the main cause of low back pain, pyroptosis is a major contributor to various diseases, including IVDD; however, there is currently no effective drugs targeting pyroptosis for therapy. In this study, we established pyroptosis model in nucleus pulposus cells (NPCs) *in vitro* and searched pyroptosis inhibitors in FDA Medicine Library. High throughput screening study revealed that Pirfenidone (PFD) was the most effective pyroptosis inhibitor among 1500+ FDA drugs, which was confirmed by further experiments. As administering PFD alone may lead to poor efficacy due to short action time and low bioavailability, we designed a smart delivery system for PFD. A pH-responsive metal-organic framework (MOF), poly-His6-zinc (PHZ) assembly, loaded with PFD (PFD@PHZ) was designed for IVDD therapy. PHZ was shown to have excellent lysosomal escape properties and bioavailability of PFD. In addition, the release of PDF from PFD@PHZ could be triggered by the acidic microenvironment of degenerated intervertebral discs. PFD@PHZ was also shown to effectively inhibit pyroptosis, senescence, and extracellular matrix (ECM) degradation in NPCs, both *in vitro* and *in vivo*, thereby mitigating the progression of IVDD in rats. Thus, the current study shows PFD as a novel inhibitor for pyroptosis, and PFD@PHZ as a potential nanomaterial for efficient IVDD therapy.

1. Introduction

Intervertebral disc degeneration (IVDD) is the main cause of low back pain, causing significant economic burden worldwide [1,2]. In anatomy, the intervertebral disc is composed of the nucleus pulposus, annulus fibrosus and cartilaginous endplate, which located between adjacent vertebral bodies [3]. Among the components of the intervertebral disc, the nucleus pulposus stands as the most essential part, primarily composed of nucleus pulposus cells (NPCs). These cells play an important role in balancing the synthesis and degradation of extracellular matrix (ECM) and maintaining the normal structure and physiology of intervertebral discs [4]. Damage and subsequent death of NPCs significantly accelerates the progression of IVDD [5,6].

Among the various forms of cell death, pyroptosis is one of the principal mechanisms contributing to the death of NPCs [7]. Pyroptosis is a lytic form of programmed cell death triggered by the activation of

* Corresponding author. Department of Orthopaedics, The Second Affiliated Hospital and Yuying Children's Hospital of Wenzhou Medical University, Wenzhou, 325088, Zhejiang Province, China.
** Corresponding author. Department of Orthopaedics, The Second Affiliated Hospital and Yuying Children's Hospital of Wenzhou Medical University, Wenzhou, 325088, Zhejiang Province, China.
*** Corresponding author. Department of Orthopaedics, The Second Affiliated Hospital and Yuying Children's Hospital of Wenzhou Medical University, Wenzhou, 325088, Zhejiang Province, China.
E-mail addresses: wuyaosen@wmu.edu.cn (Y. Wu), zhangxiaolei@wmu.edu.cn (X. Zhang), naifengtian@wmu.edu.cn (N. Tian).
[1] These authors contributed equally.

https://doi.org/10.1016/j.mtbio.2025.101729
Received 13 January 2025; Received in revised form 26 February 2025; Accepted 4 April 2025
Available online 5 April 2025

inflammasomes and caspases [8]. Unlike other forms of cell death, pyroptosis is characterized by plasma membrane rupture and the release of inflammatory mediators, which accelerate the degradation of the ECM [9]. In addition, pyroptosis is closely associated with senescence. Studies have demonstrated that the deletion of the NLRP3 inflammasome can prevent various aging-driven phenotypes [10]. In macrophage research, the activation of the pyroptosis pathway has been shown to increase with age [11]. Recent studies have revealed that NLRP3 inflammasome-mediated pyroptosis is activated in NPCs during the progression of IVDD, highlighting the significant role of pyroptosis in the IVDD procession [12]. Additionally, pyroptosis-induced senescence in NPCs can further exacerbate the progression of IVDD, creating a detrimental cycle that accelerates disc degeneration [13]. This highlights the significance of targeting pyroptosis-related pathways as a potential therapeutic strategy for mitigating IVDD.

Exploring drugs that inhibit pyroptosis in NPCs can help mitigate the progression of IVDD, which is the main purpose of our study. In previous experiments conducted by our research group, the establishment of *in vitro* cell death models, combined with high-throughput screening of drug libraries, has been validated as an efficient and precise method for identifying drugs that inhibit specific forms of cell death [14,15]. The FDA Medicine Library includes drugs that have currently passed clinical trials. These drugs have advantages such as good bioactivity and high safety. Previous studies have demonstrated that some of the FDA drugs can alleviate the progression of various diseases by inhibiting pyroptosis [16–19]. However, no studies have systematically screened for pyroptosis-inhibiting drugs within the FDA Medicine Library, and the potential of the FDA Medicine Library remains largely untapped.

We first established an *in vitro* model of pyroptosis in NPCs to conduct the screening. The combined application of lipopolysaccharide (LPS) and nigericin has been demonstrated in multiple studies to induce cellular pyroptosis [20–22]. Therefore, we selected concentrations of LPS and nigericin that resulted in a 50 % reduction in CCK8 assay outcomes compared to the control group as the stimulatory conditions to establish a model of pyroptosis in NPCs. On the basis of the successful establishment of the model *in vitro*, we introduced over 1500+ FDA drugs to attempt to rescue NPCs from pyroptosis, thereby constructing a high-throughput screening system. Finally, the rescue rate for each drug was calculated using the appropriate formula, and the drugs were ranked from highest to lowest based on their rescue rates [14]. The results indicated that pirfenidone (PFD) is the most effective drug for inhibiting pyroptosis in NPCs. PFD is a drug primarily used in the treatment of idiopathic pulmonary fibrosis, possessing anti-inflammatory, antioxidant and anti-fibrotic properties [23]. Studies have demonstrated that PFD can inhibit pyroptosis in various diseases, thereby mitigating disease progression [24,25]. However, its anti-pyroptotic effects have yet to be reported. Therefore, we selected PFD as the therapeutic agent for our study.

The delivery method of drugs is also a focus of our research. Compared to systemic administration, direct intradiscal injection of drugs helps reduce the side effects caused by systemic drug exposure and improves the efficacy of drugs [26]. However, the half-life of drugs administered within intervertebral discs is limited and requires repeated local injections, which increases the risk of secondary injury and dose-dependent side effects. Therefore, the combination of drugs and delivery platforms involving biomaterials is receiving increasing attention, as it can avoid the side effects of systemic and intradiscal administration, while enhancing the therapeutic effects of the drugs [27–29].

Nanobiomaterials have found extensive applications in biomedical domains, including biosensing, regenerative medicine, and targeted drug delivery, providing new avenues for disease treatment [30–33]. Among them, metal organic frameworks (MOFs) generated by the coordination binding of metal ions and organic ligands serve as a new type of targeted delivery biomaterial with high loading capacity and lysosomal escape characteristics, and have been widely used for drug targeted delivery and disease treatment [34,35].

In addition to traditional MOFs, certain new MOFs that can release on demand (under conditions such as pH, temperature, reactive oxygen species, etc.) have attracted great interest [36,37]. The pH value of degenerated intervertebral disc tissue decreases from 7.0 to 7.2 to 5.5–6.5, showing weak acidity [38,39]. Therefore, a pH-responsive metal-organic framework (MOF), poly-His6-zinc (PHZ) assembly, loaded with PFD (PFD@PHZ) was designed for IVDD therapy. Our study showed that the PFD@PHZ delivery system can protect NPCs from pyroptosis, senescence, and ECM degradation *in vitro* and *in vivo*, while promoting the functional recovery of IVDD. Therefore, PFD@PHZ is a new drug-loaded nanobiomaterial for treating pyroptosis, senescence, and ECM degradation of NPCs and alleviating the progression of IVDD.

2. Materials and methods

2.1. Reagents and antibodies

Pirfenidone (PFD) was acquired from MedChemExpress (Shanghai, China), type II collagenase was acquired from Sigma-Aldrich (St. Louis, Missouri, USA). Primary antibodies for β-actin, ADAMST5 and p53 were obtained from ABclonal (Wuhan, China). Primary antibodies for Collagen II, MMP13, P16, P21, ASC and NLRP3 were obtained from ABcam (Cambridge, UK). Primary antibodies for Gasdermin D and Caspase-1 were obtained from HUABIO (Hangzhou, China). Horseradish peroxidase labeled secondary antibodies, Alexa Fluor ®488 labeled sheep anti-mouse immunoglobulin (HABL) secondary antibodies was obtained from ABcam (Cambridge, UK). Reagents for cell culture were obtained from Gibco (Grand Island, NY, US).

2.2. NPCs isolation and culture

Euthanasia was performed on healthy Sprague Dawley rats (SD rats) aged 6 weeks under analgesia, and NPCs were extracted from the nucleus pulposus under sterile conditions. Collect and centrifuge, place the cell pellet in DMEM solution containing 0.025 % type II collagenase, and incubate in a humidified culture room at 37 °C and 5 % CO_2 for 6 h. Subsequently, the cells were collected again and transferred to DMEM supplemented with 10 % fetal bovine serum (FBS), 1 % penicillin, and streptomycin, and incubated in a humidified culture room at 37 °C and 5 % CO_2.

2.3. Drug-screening

LPS and nigericin were selected as inducers to establish an *in vitro* pyroptosis model. NPCs were seeded in 96-well plates at a density of 8000–10000 cells per well and cultured for 24 h. After washing with PBS, the cells were further cultured for an additional 24 h in either basal medium or basal medium supplemented with varying concentrations of LPS and nigericin. Following this incubation, the medium was replaced with 100 μL of fresh culture medium containing 10 % CCK-8. After a 2-h incubation, absorbance was measured at 450 nm using a microplate reader. The CCK-8 results were recorded, and the concentrations of LPS and nigericin were selected based on the half-maximal CCK-8 result relative to the control group treated with only basal medium. Our findings indicated that the optimal inducing concentration was 100 ng/mL of LPS and 10 μM of nigericin. Subsequently, to minimize experimental error, 100 μL of PBS was added around the perimeter of the 96-well plate. NPCs were seeded at a density of 8000–10000 cells per well and cultured for 24 h. After washing with PBS, the cells were divided into three groups: the Control group (treated with 100 μL of basal medium), the Stimulated group (treated with basal medium containing 100 ng/mL of LPS and 10 μM of nigericin), and the Drug-treated group (treated with basal medium containing 100 ng/mL of LPS, 10 μM of nigericin, and 10 μM of the drug). The cells were then incubated for an additional 24 h.CCK-8 assay was then performed to assess cell viability, and the results were recorded. The rescue rate for each drug was

calculated using the following formula: Rescue Rate = (Ac-Ab)/(Aa-Ab) * 100 %. Here Aa represents the CCK-8 test result of untreated NPCs, Ab represents the CCK-8 test result of NPCs treated with LPS and nigericin for 24 h, and Ac represents the CCK-8 result of NPCs treated with LPS, nigericin and the FDA drugs for 24 h. Finally, the rescue rates were ranked in order.

2.4. Calcein/PI staining

Inoculate NPCs at a density of 1×10^5 onto a 24 well plate, incubate for 24 h, and wash three times with PBS. Then, add PBS (control group), LPS (100 ng/ml) and nigericin (10 μM), PFD (20 μM) and PFD@PHZ (20 μM) according to different groups. After incubation for 24 h, follow the instructions and use Calcein/PI staining dye (Beyotime, Shanghai, China) to stain at 500 μL per well for 30 min, and observe under a fluorescence microscope. Viable cells exhibit green fluorescence under a fluorescence microscope, while non-viable cells exhibit red fluorescence.

2.5. Synthesis of PFD@PHZ

Poly His6 zinc assembly (PHZ) particles can be synthesized by introducing zinc ions into a His6 solution at pH 8 and subjecting it to ultrasonic treatment. Then dissolve 2 mg His6 and 2 mg PFD in 500 μL HEPES-Na buffer at pH 8.5. After 1 min of ultrasonic treatment, 24 μL of 0.1M ZnNO3 solution was introduced, followed by 15 min of ultrasonic treatment. The obtained mixture was centrifuged at 8000 rpm for 15 min, the precipitate was collected, and the particles were resuspended in 500 μL of ultrapure water. The purification process can be repeated three times to obtain PFD@PHZ.

2.6. Characterization of PHZ and PFD@PHZ

The Average size, PDI and Zeta potential of PZA and PFD@PHZ solution were determined by laser particle size analyzer (Malven Zetasizer Nano ZS90, UK). The group difference between PFD, PFD@PHZ and PHZ was detected by UV–vis spectrophotometry and ATR-FTIR spectrum. Both PHZ and PFD@PHZ solutions were deposited on copper mesh, and their respective morphologies were observed under transmission electron microscope (JEM-F200, JEOL, Japan).

2.7. Endocytosis process and mechanism of PHZ and PFD@PHZ

The NPCs were seeded at a density of 1×10^5 cells per well on a 24 well plate, incubated for 24 h, and washed three times with PBS. Subsequently, the cells were incubated in a medium containing LPS and nigericin for 24 h, followed by the addition of FITC labeled PHZ and PFD@PHZ And incubate for 2 h and 4 h respectively. After incubation, fix the cells with paraformaldehyde and perform nuclear staining with DAPI staining. Imaging was performed using a Zeiss laser scanning confocal microscope (LSM800) from Germany. Meanwhile, Lysotracker has been used for lysosome localization, providing insights into the intracellular transport of nanoparticles.

2.8. Drug release experiment of PFD@PHZ

The NPCs were seeded on a 24 well plate at a density of 1×10^5 cells per well. After incubation for 24 h, wash three times with PBS. Subsequently, the cells were treated with a medium containing LPS and nigericin and incubated for 24 h to maintain a pH of 5.5–6.5 in the medium. For drug release experiments, it will contain 1 mL PFD@PHZ Immerse the solution in 50 mL of PBS. Under the conditions of pH 6 and pH 7.2, oscillate continuously at a speed of 100 rpm for 12 h, 24 h, 2 days, 4 days, 6 days, and 8 days. Collect 1 mL of supernatant at each designated time interval and supplement with an equal amount of PBS. Use UV visible standard curve to evaluate the cumulative drug release rate at different time points.

2.9. Western blot analysis

NPCs were subjected to lysis using RIPA lysis buffer (Beyotime, China), which was supplemented with 1 mM of PMSF. The lysate was collected and then centrifuged at 12000g for 30 min at 4 °C to collect the supernatant. Subsequently, measure the protein concentration using the BCA Protein Assay Kit (Beyotime, China). Then dilute the protein to an equal concentration and volume. The same amount of protein was separated by sodium dodecyl sulfate polyacrylamide gel electrophoresis (SDS-PAGE), and then transferred to polyvinylidene fluoride (PVDF) membrane (Bio Rad, USA). After blocking the protein bands with 5 % skim milk at room temperature for 2 h, the membranes were washed three times with TBST for 10 min, and incubated with primary antibodies (1:1000): NLRP3, GSDMD, CASP-1, ASC, β-actin, Collagen II, MMP13, ADAMTS5, P16, P21, P53 overnight. Then, the membranes underwent three washes with TBST and were incubated with the appropriate secondary antibodies for a duration of 2 h. Finally, the bands were visualized using the ChemiDoc XRS + imaging system (Bio-Rad, Carlsbad, California, USA), and quantitative analysis was conducted utilizing Image Lab 3.0 software (Bio-Rad).

2.10. Molecular docking

The molecular structure of PFD can be downloaded from the PubChem database (https://pubchem.ncbi.nlm.nih.gov/). The three-dimensional structure of the large molecule NLRP3 can be downloaded from the protein database (https://www.rcsb.org/). Stable dominant conformations and molecular docking simulations can be performed using Open Babel, PyMOL, and AutoDock Tools. The results of the molecular docking simulation can be visualized using PyMOL software.

2.11. SA-β-gal staining

According to the instructions, the senescence related β-galactosidase (SA-β-gal) staining kit (Beyotime, Shanghai, China) was used to stain the NPCs, and observed under an optical microscope. The senescent NPCs appeared blue.

2.12. Immunofluorescence

Plant NPCs at a density of 1×10^5 cells per well into a 24 well plate and culture for 24 h. After group pretreatment, fix with 4 % paraformaldehyde for 15 min, wash three times with PBS, and then permeate with 0.1 % Triton X-100. Subsequently, the primary antibody (diluted 1:100) was mixed with 10 % FBS and incubated with cells for 24 h. Subsequently the cells were incubated with Alexa Flour 488 conjugated secondary antibody (Jackson ImmunoResearch, West Grove, USA) in the dark for 2 h, followed by incubation with DAPI for 5 min, washing, and then observing and collecting images using a laser scanning confocal microscope (Zeiss) to quantify fluorescence intensity and analyze the results.

2.13. Animal models

Select 8-week-old SD rats and randomly divide them into five groups, with five animals in each group: Sham surgery group, IVDD group, IVDD + PHZ group, IVDD + PFD group, and IVDD + PFD@PHZ group. Animals are kept in clean rooms at 24–26 °C, under a 12 h cycle of darkness/light, and provided with water and food at will. For the experimental group that requires modeling, a needle (21G) is used to completely penetrate the fibrous ring from the tail skin. Then rotate the needle 360°and let it sit for 1 min. In IVDD + PHZ group, IVDD + PFD and IVDD + PFD@PHZ group, the drug was administered via

intervertebral disc injection at a concentration of 20 μM, with a volume of 5 μL injected weekly. Both Sham group and IVDD group were injected with the same volume of physiological saline. After four and eight weeks, all rats were euthanized.

2.14. X-ray imaging and magnetic resonance imaging (MRI)

At 4 and 8 weeks after the establishment of the IVDD model, all rats were anesthetized and X-ray imaging (KUB Technologies Inc.) was performed. The heights of the intervertebral discs for each group were then quantified using the Disc Height Index (DHI) [40]. MRI was performed utilizing a Bruker BioSpec 94/20 USR MRI system (Bruker, Germany) to evaluate the degrees of IVDD in accordance with the Pfirrmann classification system.

2.15. Histology and immunohistochemistry

After euthanasia of rats, intervertebral disc tissue was separated and fixed in 4 % paraformaldehyde for 48 h, then decalcified in EDTA solution and embedded in paraffin. Cut the tissue slices into 3 μm sections and stain them with safranin O-fast green (SO). Observe histopathological images of tissues under a microscope (Nikon, Japan) and evaluate them by independent researchers who are not familiar with treatment conditions. In addition, immunohistochemical staining was performed on rat intervertebral disc slices to detect the presence of the aforementioned proteins and observe their changes, and corresponding quantification was performed using Image J software.

2.16. Immunohistochemical (IHC) analysis

Remove the prepared tissue slices by dewaxing in xylene. Subsequently, immerse it in 3 % H2O2 for 10 min. Then use citrate buffer for antigen repair. Seal the sections with 10 % goat serum for 1–2 h and incubate overnight at 4 °C with primary antibody diluted according to their characteristics. Subsequently, the slices were incubated with the corresponding secondary antibody at 37 °C for 2 h. After incubating with SABC working solution at room temperature for 1 h, perform DAB staining and counterstain with hematoxylin. Capture images using an Olympus fluorescence microscope (Olympus, Tokyo, Japan) and analyze them using Image J software 2.1 (Bethesda, Maryland, USA).

2.17. Immunofluorescence (IF) analysis

The tissue slices were deparaffinized in xylene and hydrated in ethanol. Subsequently, immerse it in 3 % hydrogen peroxide for 10 min. Then use citrate buffer for antigen repair. Seal the sections with 10 % goat serum for 1–2 h and incubate overnight at 4 °C with primary antibody diluted according to its characteristics. After washing three times with PBS, the cells were incubated with Alexa Fluor488 secondary antibody (diluted 1:100) at room temperature for 2 h, and then washed three times with PBS. Finally, the cells were stained with DAPI for 10 min. Fluorescence images were acquired using a fluorescence microscope (Olympus, Tokyo, Japan), and Image J software 2.1 (Bethesda, MD, USA) was used for fluorescence result analysis.

2.18. Statistical analysis

SPSS 19.0 (SPSS, Chicago, IL) was used for all statistical analyses. The mean and Standard Error of Mean (SEM) for all data are displayed. One-way ANOVA or the *t*-test were used to determine whether there were any differences between the groups. Statistical significance was defined as $P < 0.05$.

3. Results

3.1. Screening for the FDA Medicine Library of pyroptosis inhibitor

Fig. 1A shows the drug screening process in the FDA Medicine Library. We established a model of pyroptosis in NPCs *in vitro* induced by LPS (100 ng/ml) and nigericin (10 μM). Subsequently, we added different drugs (10 μM) from the FDA Medicine Library to select drugs that could inhibit pyroptosis in NPCs. Then, we used the CCK8 assay to evaluate the survival rate of the cells and ranked them based on their rescue rate (RR). Fig. 1B shows the RR of various drugs in NPCs under the action of pyroptosis inducers. Among them, PFD has the highest RR, so we choose PFD as the drug to inhibit pyroptosis in NPCs. Fig. 1C shows the structural formula of PFD.

Subsequently, we evaluated the cytotoxicity of PFD. The results showed that PFD had no cytotoxicity at concentrations of 5, 10, and 20 μM, but had significant cytotoxicity at a concentration of 40 μM (Fig. 1D). Meanwhile, in order to further evaluate the therapeutic potential of PFD, we studied the therapeutic effect of different concentrations of PFD under the action of pyroptosis inducing agents. The results, as shown in Fig. 1E, demonstrated that the therapeutic effect of PFD was optimal at a drug concentration of 20 μM. Subsequently, we further validated the therapeutic effect of PFD using Calcein/PI staining, and the results showed that PFD could effectively inhibit pyroptosis in NPCs (Fig. 1F and G).

Subsequently, we performed western blot to verify the changes in pyroptosis-related proteins. NLRP3 is a key protein involved in the formation of the inflammasome during pyroptosis. Upon stimulation with LPS and nigericin, NLRP3 is activated, recruiting the adaptor protein ASC and the protease pro-caspase-1 to form a macromolecular complex. This complex cleaves pro-caspase-1 (Pro-CASP-1) into its active form, cleaved-caspase-1 (C-CASP-1). Activated caspase-1 subsequently cleaves gasdermin D (GSDMD), generating GSDMD-N, which forms pores in the host cell membrane to regulate the release of cytoplasmic contents, ultimately leading to cell pyroptosis. The results are shown in Fig. 1H–I. The protein amounts of NLRP3, GSDMD-N, C-CASP-1 and ASC in NPCs were significantly increased by LPS + Nigericin stimulation, but decreased significantly after treatment with PFD, indicating that PFD can well inhibit pyroptosis of NPCs.

In summary, through drug screening in FDA Medicine Library, it is found that PFD can effectively inhibit LPS- and migericin-induced pyroptosis of NPCs.

3.2. Synthesis and characterization of PFD@PHZ

In order to enhance the therapeutic effect of PFD, we synthesized the nano material PHZ, which is a novel metal organic material, and encapsulated PFD into PHZ to form a new nano drug named PFD@PHZ.

In an environment of pH-8.5, the coordination interaction between poly-His6 molecules and Zn^{2+} produces PHZ, and then PFD is encapsulated in PHZ to form PFD@PHZ (Fig. 2A). The size distribution and zeta potential of PFD@PHZ were tested by dynamic light scattering (DLS). The average size of PFD@PHZ is slightly lower than that of PHZ. The Polydispersity index (PDI) is the dimensionless constant that reflects the particle size distribution width. The smaller the value, the more uniform the particle size and the more concentrated the distribution. The PDI of PFD@PHZ is slightly smaller than PFD, indicating the particle size of PFD@PHZ is relatively concentrated. At the same time, the zeta potential of the PFD@PHZ is 30.6 mV, which has good stability. (Fig. 2B).

Subsequently, as shown in Fig. 2C, we found through UV–visible spectrum analysis that a strong absorption peak with a wavelength of 298 nm in the UV spectrum of PFD, which is the characteristic absorption peak of the benzene ring in PFD. And in PFD@PHZ, the characteristic peak of the benzene ring significantly weakened and shifted, appearing at 308 nm, indicating successful encapsulation of PFD by

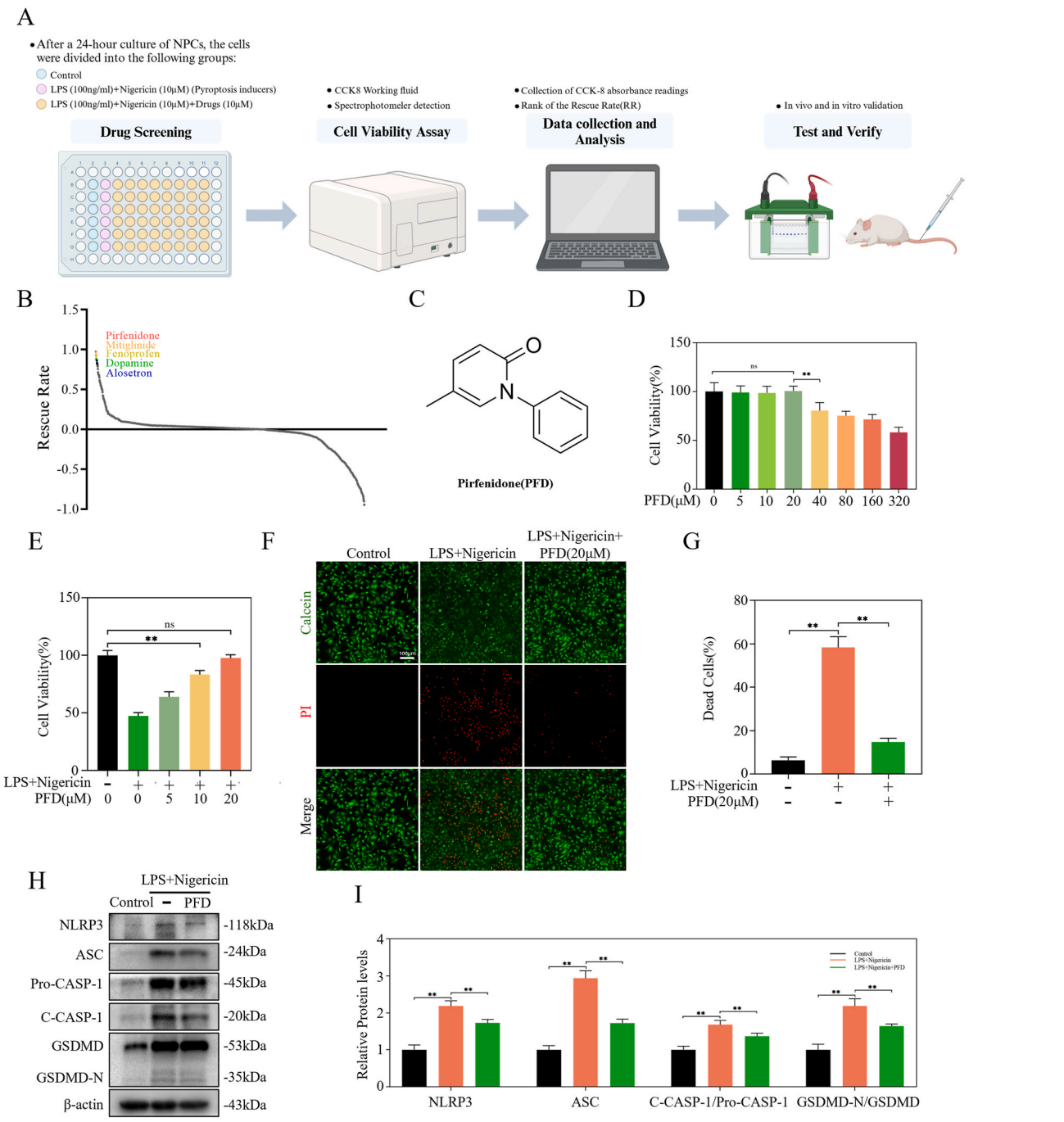

Fig. 1. Screening for the FDA Medicine Library of pyroptosis inhibitor (A) Drug screening process in the FDA Medicine Library. (B) Screening results from the FDA Medicine Library. Rescue Rate = (Ac-Ab)/(Aa-Ab) * 100 %. Here Aa represents the CCK-8 test result of untreated NPCs, Ab represents the CCK-8 test result of NPCs treated with LPS and nigericin for 24 h, and Ac represents the CCK-8 result of NPCs treated with LPS, nigericin and the FDA drugs for 24 h (n = 3). (C) The chemical molecular formula of PFD. (D) NPCs treated with different doses of PFD for 24 h (n = 3). (E) Pyroptosis-induced NPCs treated with different doses of PFD (n = 3). (F–G) Calcein/PI detection in the above-mentioned treated NPCs (scale bar: 100 μm; n = 3). (H–I) Protein expression of NLRP3, ASC, C-CASP-1 and GSDMD-N was analyzed by western blot in NPCs treated with LPS and nigericin in the presence or absence of 20 μM PFD (n = 3). Data are shown as the mean value (n = 3) ± S.D. Statistical significance is denoted by $^{**}p < 0.01$,$^{*}p < 0.05$.

PHZ. Also, the infrared spectra of PFD, PHZ, and PFD@PHZ can be seen from the infrared spectra (Fig. 2D). Among them, 3340 cm^{-1} is the stretching vibration absorption peak of N-H on PHZ, 1673 cm^{-1} is the stretching vibration absorption peak of C=C double bond and (amide I band) C=O on PFD, 1610-1453 cm^{-1} is the skeleton vibration absorption peak of benzene ring on PFD, and 825-699 cm^{-1} is the out of plane bending vibration absorption peak of C-H on PFD. The results showed that PHZ successfully encapsulated PFD. Meanwhile, as shown in Fig. 2E, under SEM, the nanoparticles of PHZ and PFD@PHZ exhibit an irregular but uniformly distributed morphology.

In summary, the above experimental results clarify the PFD@PHZ is successfully synthesized and supported its functionality in subsequent applications.

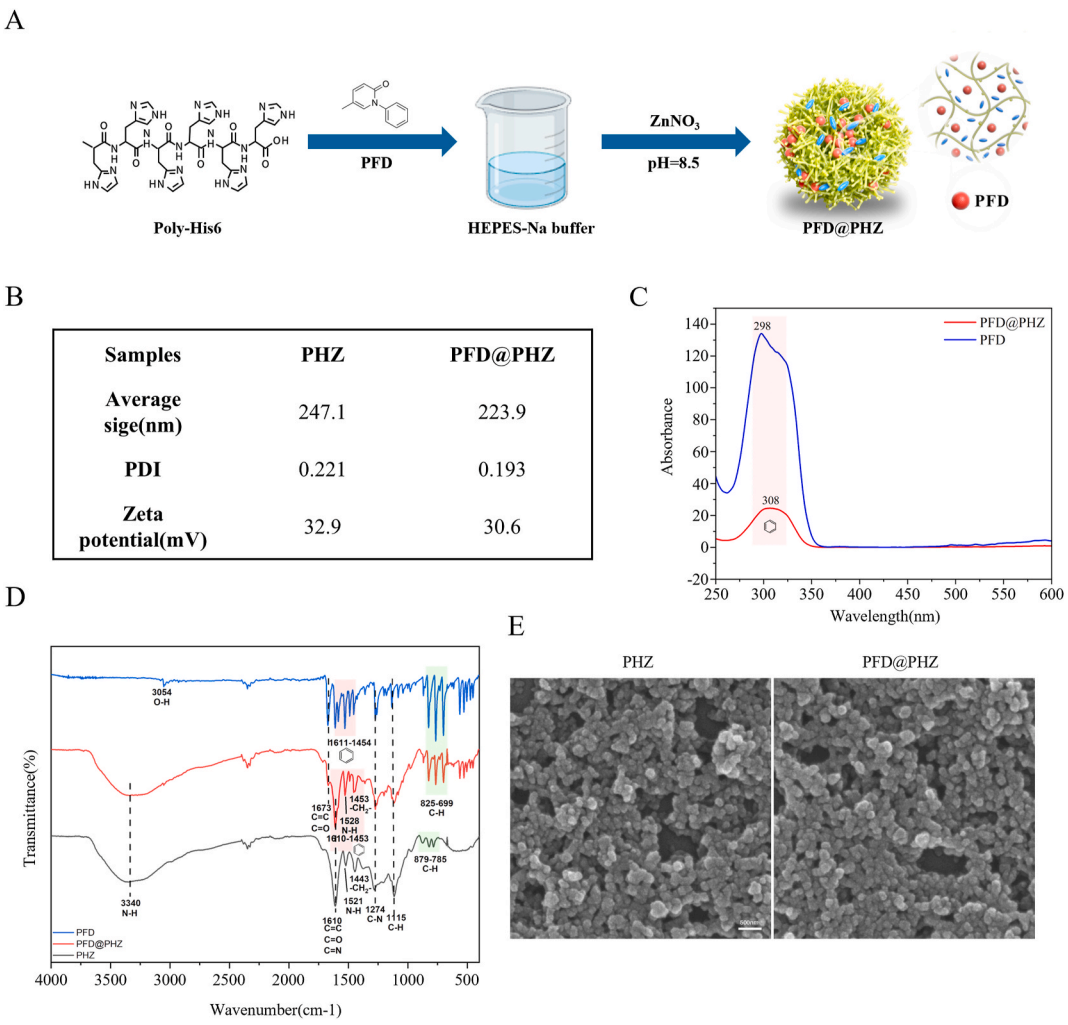

Fig. 2. Synthesis and characterization of PFD@PHZ (A) Synthesis of PFD@PHZ. (B)Average sige, PDI and Zeta potential of PHZ and PFD@PHZ (n = 3). (C) The UV–visible spectrum analysis of PFD and PFD@PHZ. Blue represents PFD, and red represents PFD@PHZ. (D) The infrared spectra of PFD, PHZ and PFD@PHZ. Blue represents PFD, red represents PFD@PHZ and black represents PHZ. (E) SEM of PHZ and PFD@PHZ (n = 3).

3.3. In vitro cytotoxicity assessment, cellular uptake and drug release studies of PFD@PHZ

The aforementioned experiments successfully confirmed the synthesis of PFD@PHZ. Next, further investigations will be conducted to assess its toxicity, cellular uptake, and biocompatibility in NPCs.

We use different concentrations of PFD@PHZ to stimulate the NPCs and detect cellular activity using CCK8. As shown in Fig. 3A, at a concentration of 5, 10, 20 μM, PFD@PHZ does not cause toxicity to cells, but when the concentration is increased to 40 μM, cellular activity significantly decreases. Therefore, we chose concentrations of 5, 10 and 20 μM PFD@PHZ to explore its ability to rescue NPCs under pyroptosis inducers. As shown in Fig. 3B, a concentration of 20 μM PFD@PHZ was most effective in rescuing NPCs from pyroptosis. Additionally, we divided the NPCs into three groups: “PBS”, “LPS + Nigericin”, and “LPS + Nigericin + PFD@PHZ”. Equal amounts of the respective reagents were added to each group, with PFD@PHZ at a concentration of 20 μM, followed by calcein/PI staining. As shown in Figs. 3C and 20 μM PFD@PHZ will not cause the death of NPCs and can effectively rescue NPCs stimulated by pyroptosis inducers. The above results demonstrated that PFD@PHZ has good biocompatibility and pyroptosis rescue ability at a concentration of 20 μM.

At the same time, in order to verify the drug delivery capability of PHZ, we have developed the PFD-FITC@PHZ and PFD-FITC. Equal concentrations of reagents have been added to two groups of cells and the fluorescence images were captured after 4 h. The stronger the green fluorescence, the more drug enters the cell. As shown in Fig. 3D, the amount of drugs entering the cells in the PFD-FITC@PHZ group was significantly higher than that in the PFD-FITC group, indicating the PFD@PHZ can promote the entry of drugs into cells.

To verify the cellular uptake of PHZ and PFD@PHZ, equal amount of PHZ-FITC and PFD@PHZ-FITC was added to two groups of cells separately. Fluorescence imaging was performed after 2 and 4 h, and the results were shown in Fig. 3E. PHZ and PFD@PHZ entered the cells in the form of relatively dense clumps and then gradually dispersed in the cells. In order to further clarify the intracellular localization of drug delivery, we treated two groups of cells with PHZ-FITC and PFD@PHZ-FITC respectively, and used Lysotracker to stain lysosomes. The results are presented in Fig. 3F, which showed only a small overlap between the two fluorescent colors, indicating that PHZ and PFD@PHZ can effectively escape lysosomal phagocytosis and exert their effects within cells.

Next, we assess the controlled drug release of PHZ in acidic environments. Fig. 3G shows the percentage change of drug release from PFD@PHZ over time under different pH environments. The results demonstrated that the drug release is rapid within 1 day, and then the drug release rate slows down. It can also be demonstrated that lower pH values can lead to faster drug release and higher cumulative release (22 % release at pH = 7.2 and 84.7 % release at pH = 6.0). At the same time,

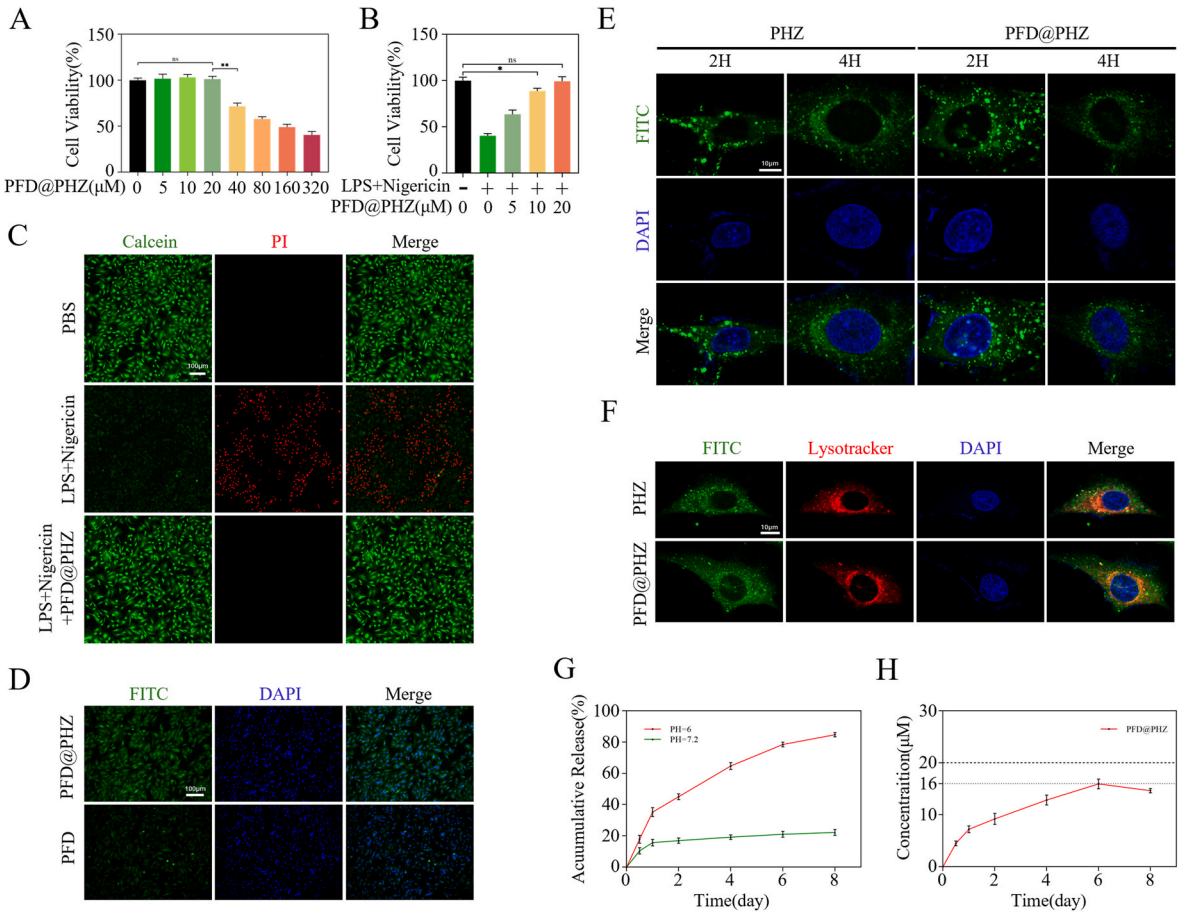

Fig. 3. *In vitro* cytotoxicity assessment, cellular uptake and drug release studies of PFD@PHZ (A) NPCs treated with different doses of PFD@PHZ for 24 h (n = 3). (B) Pyroptosis-induced NPCs treated with different doses of PFD (n = 3). (C) Calcein/PI detection in the above-mentioned treated NPCs (scale bar: 100 μm; n = 3). (D) Fluorescence images of NPCs after 4 h of PFD-FITC@PHZ and PFD-FITC treatment, respectively (scale bar: 100 μm; n = 3). (E) Fluorescence images of NPCs after 2 h and 4 h treatment with PHZ-FITC and PFD@PHZ-FITC, respectively (scale bar: 10 μm; n = 3). (F) Fluorescence images of NPCs after treatment with PHZ-FITC, PFD@PHZ-FITC, and Lysotracker, respectively (scale bar: 10 μm; n = 3). (G) The percentage change of drug release from PFD@PHZ over time under different pH environments. Red represents at pH = 6 and green at pH = 7.2 (n = 3). (H) The percentage change of drug release from PFD@PHZ over time at pH = 6. Red represents PFD@PHZ. Data are shown as the mean value (n = 3) ± S.D. Statistical significance is denoted by**p < 0.01, *p < 0.05.

as shown in Fig. 3H, in an environment of pH = 6.0, the concentration of PFD is within the therapeutic window and can exert an effective therapeutic effect within 7 days.

The above results verify that PFD@PHZ had no biological toxicity and possess multiple capabilities such as lysosomal escape, rapid intracellular drug delivery, and controlled drug release.

3.4. PFD@PHZ inhibits pyroptosis in NPCs

As shown in Fig. 4A, exogenous stimuli, including LPS and nigericin, can induce inflammatory responses and degenerative phenotypes of NPCs by increasing reactive oxygen species (ROS) production and activating NLRP3. Simultaneously, the generated ROS can also activate NLRP3, further promoting pyroptosis in NPCs.

To verify the therapeutic effect of PFD@PHZ, we used DCFH-DA reactive oxygen species ROS probe to detect the content of ROS in NPCs. It was found that LPS and nigericin stimulation can significantly increase the content of ROS, while treatment with PFD can reduce the content of ROS. Compared with the therapeutic effect of PFD, treatment with PFD@PHZ can further reduce the content of ROS (Fig. 4B). Subsequently, changes in pyroptosis-related proteins were detected by western blot. Fig. 4C–D showed that NLRP3, GSDMD-N, C-CASP-1 and ASC were significantly increased under the stimulation of LPS and melanocortin, and both PFD and PFD@PHZ treatments could reduce the above-mentioned protein content, it is worth noting that PFD@PHZ has a more significant effect on reducing the above-mentioned protein content. Subsequently, we supplemented the cell fluorescence of NLRP3, and as shown in Fig. 4E–F, PFD@PHZ had a better therapeutic effect in reducing the NLRP3 content than PFD. At the same time, it has been documented that PFD can inhibit the activation of NLRP3 inflammatory factors [41]. To verify the interaction between PFD and NLRP3, docking analysis was performed using the AutoDock tool. The docking results showed that PFD and NLRP3 formed a stable hydrogen bond on TYR-381 (Fig. 4G). This suggests that PFD may interact with NLRP3 under specific conditions.

In summary, stimulation with LPS and nigericin induces pyroptosis in NPCs, while both PFD and PFD@PHZ exhibit the ability to inhibit this process, with PFD@PHZ demonstrating a more pronounced therapeutic effect.

3.5. PFD@PHZ inhibits senescence in NPCs

Pyroptosis may also lead to cellular senescence. Thus, subsequent experiments were further carried out to investigate the anti-senescence effects of PFD@PHZ.

First, changes in senescence-related indicators were detected by western blot, and it was found that the levels of senescence-related proteins such as p16, p21 and p53 increased significantly under the stimulation of LPS and nigericin. Under PFD treatment, the above-mentioned related indicators decreased, and the treatment effect of

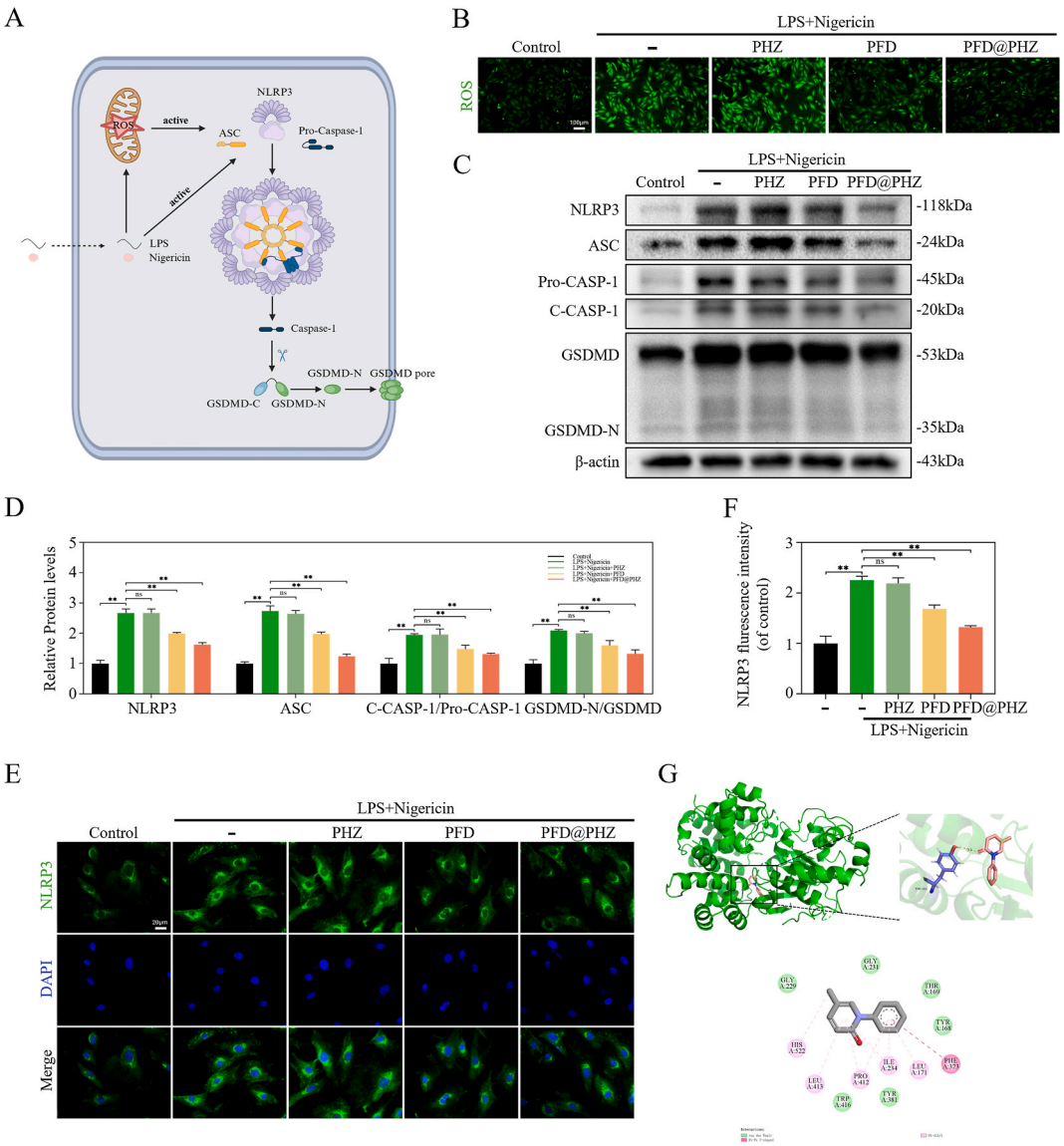

Fig. 4. PFD@PHZ inhibits pyroptosis in NPCs (A) LPS and nigericin induce ROS production and pyroptosis. (B) Measurement of ROS content in NPCs (scale bar: 100 μm; n = 3). (C–D) Western blot of NLRP3, ASC, C-CASP-1 and GSDMD-N of NPCs in different treatment groups (n = 3). (E–F) Immunofluorescence images of NLRP3 of NPCs in different treatment groups (scale bar: 20 μm; n = 3). (G) The binding site for NDGA and Nrf2. All data are presented as the mean ± SD. Data are shown as the mean value (n = 3) ± S.D. Statistical significance is denoted by**p < 0.01, *p < 0.05.

PFD@PHZ was more significant (Fig. 5A–B). Cell fluorescence results were consistent with western blot (Fig. 5C–D). Then senescence-related β-galactosidase staining was used to detect the senescence of NPCs. The results showed that blue precipitates appeared in the NPCs under the stimulation of LPS and nigericin. Both PFD and PFD@PHZ treatments can reduce the number of senescent cells, and the treatment effect of PFD@PHZ is more significant (Fig. 5E–F).

In summary, LPS and nigericin stimulation can cause the senescence of NPCs, while PFD and PFD@PHZ can inhibit the senescence of NPCs. At the same time, PFD@PHZ has a more significant inhibitory effect on senescence.

3.6. PFD@PHZ inhibits ECM degradation in NPCs

The most noticeable change in IVDD is the degradation of the ECM. In order to verify the therapeutic effect of PFD@PHZ in NPCs, we tested its function of alleviating ECM degradation.

As shown in Fig. 6A–B, the results of western blot showed that under the stimulation of LPS and nigericin, collagen II was significantly reduced, and MMP13 and ADAMST5 were significantly increased. The use of PFD inhibited this trend, and the inhibitory effect of PFD@PHZ was more obvious. As shown in Fig. 6C–D, the trend of cell immunofluorescence was consistent with that of western blot. In addition, in order to show the content of proteoglycan in NPCs, we performed toluidine blue staining. As shown in Fig. 6E–F, under the induction of LPS and nigericin, the ECM of NPCs was degraded, and the degradation of ECM was inhibited after treatment with PFD, and the effect was more significant after treatment with PFD@PHZ.

In conclusion, PFD can suppress ECM degradation of NPCs, while PFD@PHZ is more effective to decrease ECM degradation of NPCs.

3.7. PFD@PHZ inhibits the progression of IVDD in rats

To evaluate the therapeutic effects of PFD and PFD@PHZ *in vivo*, we utilized the rat disc puncture model, which is a commonly used animal model in IVDD research [40]. The results showed that PFD and PFD@PHZ could effectively alleviate IVDD without toxicity to other organs of rats (Fig. S1).

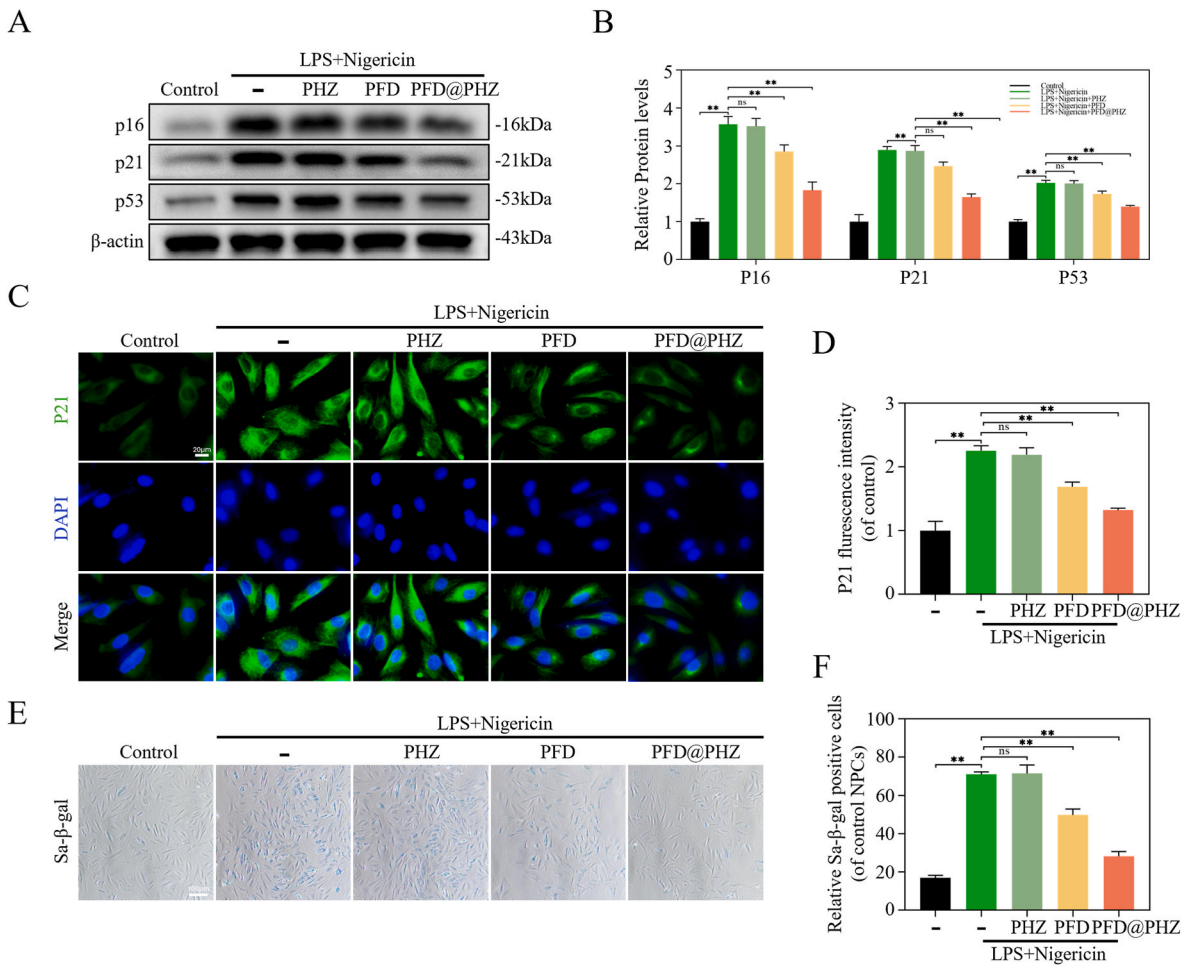

Fig. 5. PFD@PHZ inhibits senescence in NPCs (A–B) Western blot of P16, P21 and P53 of NPCs in different treatment groups (n = 3). (C–D) Immunofluorescence images of P21 of NPCs in different treatment groups (scale bar: 20 μm; n = 3). (E–F) SA-β-gal images of NPCs in different treatment groups (scale bar: 100 μm; n = 3). Data are shown as the mean value (n = 3) ± S.D. Statistical significance is denoted by **p < 0.01, *p < 0.05.

According to the X-ray results, compared with the sham group, the intervertebral disc height index (DHI) of the IVDD group and IVDD + PHZ group was significantly lower. At the same time, it can be seen that the tissue DHI after 8 weeks of modeling was lower than that after 4 weeks of modeling. In the IVDD + PFD group at 4w and 8w, it can be seen that DHI recovered, while in the IVDD + PFD@PHZ group, DHI recovered further. This showed that PFD@PHZ can further alleviate the progression of IVDD by exerting the release and delivery function of drugs. In addition, we used MRI to evaluate the degree of IVDD by Pfirrmann score. The results showed that the Pfirrmann scores of the IVDD group and the IVDD + PHZ group were significantly higher than those of the sham group, and the Pfirmann score of the IVDD + PFD group was reduced, and the Pfirmann score of the IVDD + PFD@PHZ group was reduced more significantly. At the same time, it can be seen that the 8w treatment effect of PFD@PHZ is better than that of 4w (Fig. 7B–D).

Next, we further evaluated the histological changes of the intervertebral disc by tissue sections. As shown in Fig. 7E–F, in the IVDD group and IVDD + PHZ, obvious nucleus pulposus tissue loss and intervertebral disc fibrosis were observed, while PFD administration alleviated IVDD progression, and PFD@PHZ administration had a better therapeutic effect than PFD alone (Fig. 7E–F).

Subsequently, pyroptosis and ECM-related indicators were detected by immunohistochemical staining. We found that with the progression of IVDD, the expression of NLRP3 increased significantly, and the use of PFD could inhibit the increased expression of NLRP3 in the nucleus pulposus tissue. At the same time, due to the intracellular delivery and extracellular controlled release of PHZ, the expression of NLRP3 in PFD@PHZ further decreased compared with the PFD group, and the decrease was more significant at 8w (Fig. 7G–H). As IVDD progresses, the expression of Collagen II decreases significantly, and the use of PFD can inhibit the decrease in Collagen II expression in the nucleus pulposus tissue. At the same time, compared with the PFD group, the expression of Collagen II in PFD@PHZ further increased, and the increase was more significant at 8w (Fig. 7I–J). The above results show that PFD@PHZ can well inhibit pyroptosis and ECM degradation in rat nucleus pulposus tissue.

At the same time, we performed tissue fluorescence staining, and the results were shown in Fig. 8A–I. In the IVDD and IVDD + PHZ groups, with the progression of IVDD, the protein expression of NLRP3, P16 and ADAMTS5 increased, while the expression of the above proteins decreased after treatment with PFD and PFD@PHZ. Among them, the protein expression decreased more significantly after PFD@PHZ treatment. At the same time, the treatment effect of 8w was better than that of 4w.

In conclusion, the use of PFD and PFD@PHZ can improve the recovery of the function and structure of degenerated intervertebral discs while inhibiting the pyroptosis, senescence, and ECM degradation of nucleus pulposus tissue, and PFD@PHZ has a better therapeutic effect.

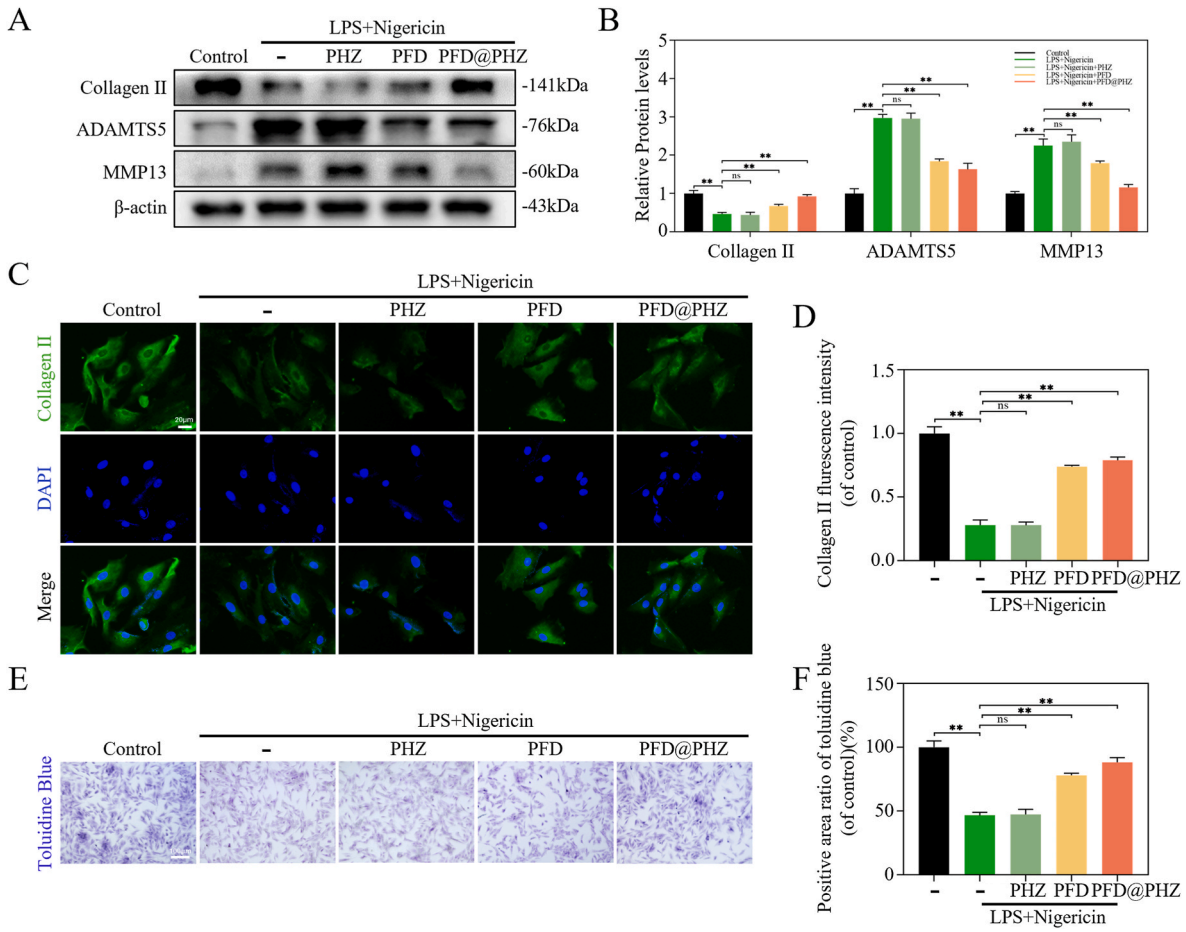

Fig. 6. PFD@PHZ inhibits ECM degradation in NPCs (A–B) Western blot of Collagen II, ADAMTS5 and MMP13 in NPCs in different treatment groups (n = 3). (C–D) Immunofluorescence images of Collagen II of NPCs in different treatment groups (scale bar: 20 μm; n = 3). (E–F) Toluidine Blue images of NPCs in different treatment groups (scale bar: 100 μm; n = 3). Data are shown as the mean value (n = 3) ± S.D. Statistical significance is denoted by**p < 0.01, *p < 0.05.

4. Discussion

IVDD is one of the most prevalent degenerative spinal disorders, significantly impacting quality of life and imposing substantial social and economic burdens [42]. Pathologically, IVDD is characterized by nuclear dehydration, annular fissures and the formation of cartilage endplate cracks [43]. As the disease progresses, it increasingly affects patients' quality of life, with primary symptoms including chronic low back pain, restricted mobility, limb numbness, and weakness, potentially leading to disability [44]. Multiple risk factors contribute to IVDD, including aging, prolonged poor posture and genetic predisposition. Current research suggests that the progression of the disease is primarily attributed to the senescence and death of NPCs and an imbalance between the synthesis and degradation of the ECM [45].

Cell death can occur in various forms, including apoptosis, pyroptosis, ferroptosis and cuproptosis [46]. Upon exposure to diverse stimuli, one or more of these forms of cell death may be triggered, thereby promoting the progression of IVDD. Pyroptosis represents a newly identified form of programmed cell death that plays a significant role in nucleus pulposus cell demise [47]. This process is characterized by the formation of membrane pores, the release of pro-inflammatory cytokines, and cellular lysis. The mechanisms underlying pyroptosis are intricate, encompassing both classical and non-classical pathways [48]. In the classical pyroptotic pathway, activation of inflammasomes, primarily NLRP3, leads to the cleavage of Pro-Caspase-1 into its active form, Caspase-1. Caspase-1 then cleaves GSDMD to generate active N- and C-terminal fragments, with the N-terminal fragment facilitating membrane pore formation and driving cell death. In contrast, the non-classical pathway of pyroptosis is mediated by Caspase-4, Caspase-5, and Caspase-11, which induce membrane pore formation, cellular lysis, and subsequent inflammatory responses. These diverse pathways collectively contribute to pyroptosis, and its inhibition represents a critical strategy for reducing nucleus pulposus cell death and alleviating the progression of IVDD [49].

Pharmacological intervention is a commonly employed approach for the treatment of IVDD [50]. However, current drug therapies primarily focus on symptom alleviation and functional improvement, without fundamentally reversing the progression of disc degeneration. Consequently, the identification of a therapeutic agent capable of mechanistically inhibiting NPCs death and mitigating the progression of IVDD is of paramount importance. We have selected the FDA Medicine Library for screening, not only due to its proven bioactivity and high safety profile, but also because existing studies have demonstrated that compounds from this library can inhibit pyroptosis [16–18]. This provides a solid foundation for our research. In our study, we first induced pyroptosis in NPCs *in vitro* using LPS and nigericin, establishing an pyroptosis model *in vitro*, and then tested the therapeutic potential of 1500+ drugs from the FDA Medicine Library. Our study realved that PFD is the most effective agent for inhibiting pyroptosis. Previous research has also shown that PFD exerts a protective effect by inhibiting pyroptosis in various diseases [51,52], yet its application in IVDD remains unexplored. Therefore, we have chosen PFD as the focal point of our investigation, aiming to prevent pyroptosis and mitigate the progression of IVDD.

However, the effectiveness of using drugs alone to treat IVDD is limited. Thus, we designed a drug-controlled release delivery system to

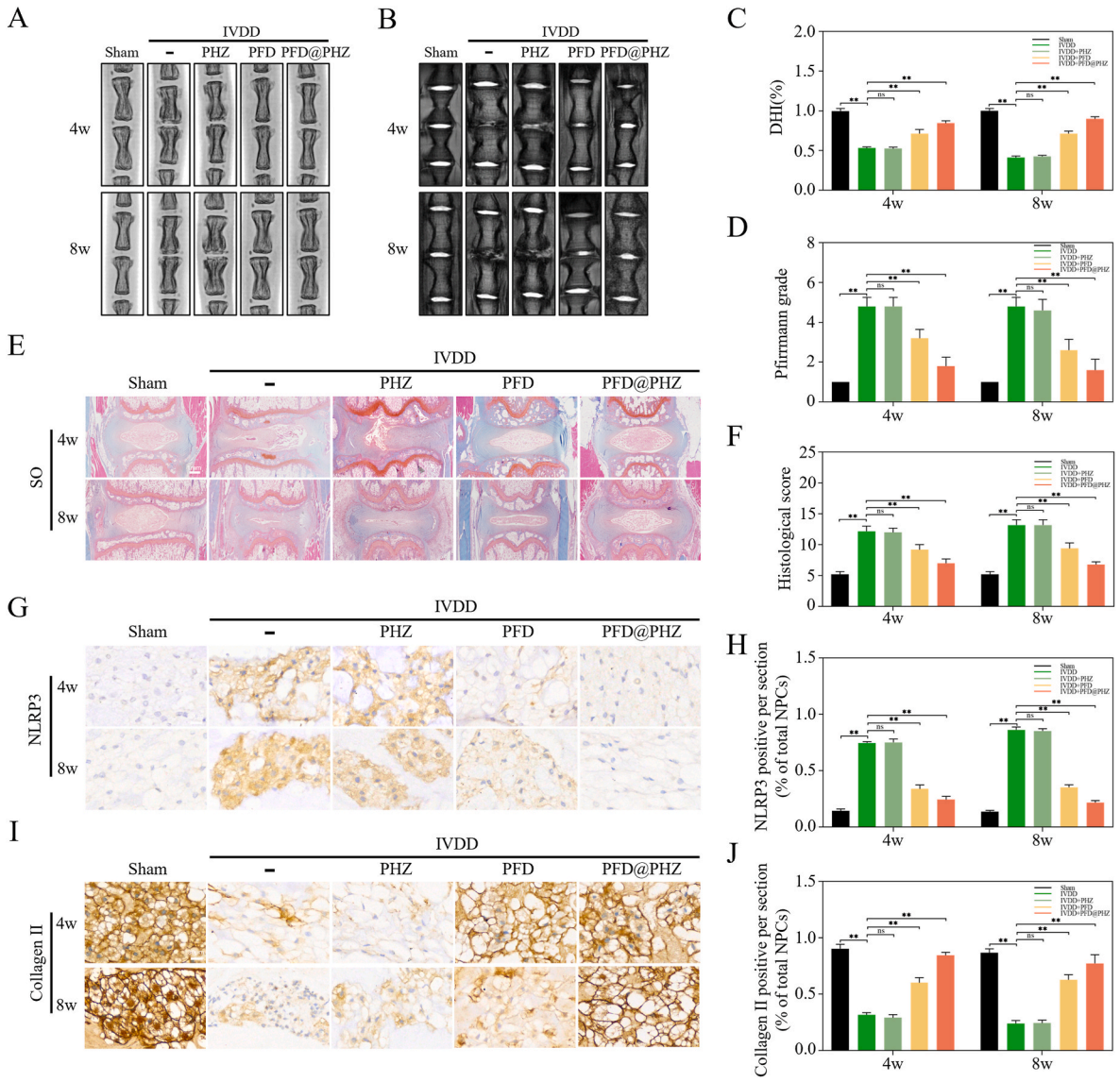

Fig. 7. PFD@PHZ inhibits the progression of IVDD in rats (A, C) Representative X-ray image and Disc Height Index (DHI) measurement of a rat tail disc 4 weeks and 8 weeks after disc puncture surgery (n = 5). (B, D) MRI and Pfirrmann score assessment of rat tails at 4 weeks and 8 weeks after disc puncture surgery (n = 5). (E–F) Evaluation of histological grades at 4 weeks and 8 weeks post-surgery (scale: 1 mm). (G–H) Evaluation of NLRP3 expression in discs through immunohistochemical staining (scale: 20 μm; n = 5). (I–J) Evaluation of Collagen II expression in discs through immunohistochemical staining (scale: 20 μm; n = 5). Data are shown as the mean value (n = 3) ± S.D. Statistical significance is denoted by $^{**}p < 0.01$,$^{*}p < 0.05$.

maximize the therapeutic potential of PFD. Moreover, upon disc degeneration, the microenvironment within the disc undergoes an acidic shift, characterized by a reduced pH [53,54], which provided the conceptual foundation for our material targeting strategy. To optimize both drug release and therapeutic efficacy, we developed a zinc histidine-based assembly (PHZ) and efficiently encapsulated PFD within PHZ, yielding the PFD@PHZ. Our study demonstrates that PFD@PHZ is synthesized through a simple process and exhibits several key characteristics, including lysosomal escape, efficient drug delivery, sustained release and pH-targeted properties. Additionally, we confirmed that a concentration of 20 μM PFD@PHZ is non-toxic to cells and effectively inhibits NPCs pyroptosis both *in vitro* and *in vivo*, thereby alleviating IVDD. Further investigation revealed that PFD@PHZ not only mitigated pyroptosis in NPCs but also suppressed oxidative stress, cellular senescence and ECM degradation, offering multi-faceted protection against NPCs death and demonstrating exceptional therapeutic efficacy.

Our research has demonstrated that PFD@PHZ is an effective drug-delivery material for alleviating IVDD, offering significant advantages. However, despite these promising findings, there are still limitations in the current study.

Drug screening is an effective strategy for targeting diseases and selecting therapeutic agents, and has been widely applied in various studies [55]. Although our screening approach enables the precise identification of drugs that inhibit specific forms of cell death, several challenges remain, including issues such as drug failure, varying optimal concentrations for different drugs and a limited variety of drugs available for selection. In contrast to our current method, Surface Plasmon Resonance (SPR) drug screening is increasingly capturing the attention of researchers [56,57]. SPR screening follows a three-step approach—Clean Screen, Binding Level Screen, and Affinity Screen—which allows for the coarse screening, fine screening, and affinity characterization of drug libraries [58]. This method expands the range of drug candidates and enables the selection of drugs that best meet specific needs, while also facilitating the identification of compounds with optimal affinity. Therefore, we plan to incorporate SPR screening technology into our future screening strategies, aiming to identify target

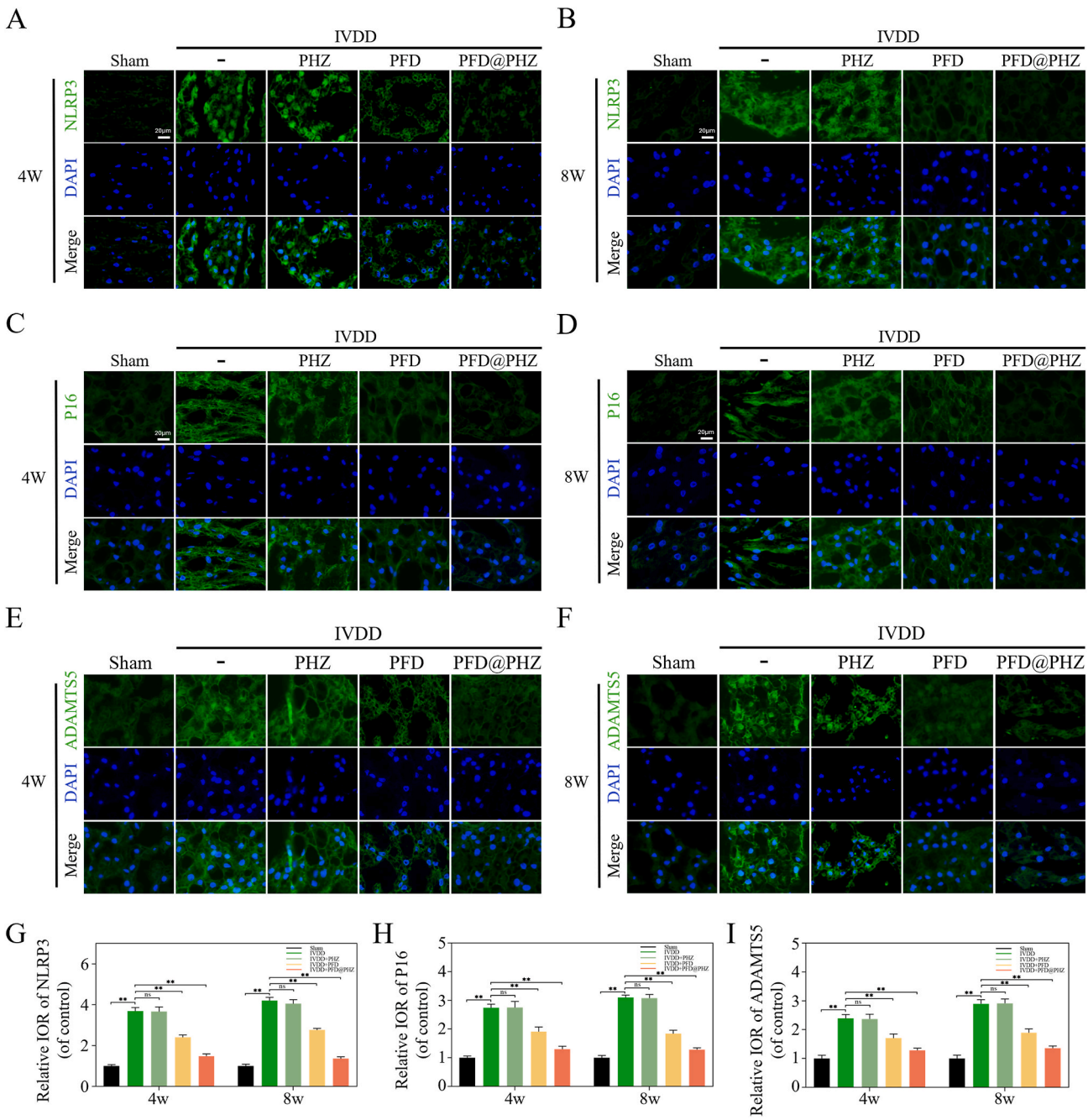

Fig. 8. Tissue immunofluorescence shows PFD@PHZ inhibits the progression of IVDD in rats (A-B, G) Evaluation of NLRP3 expression in discs through tissue immunofluorescence (scale: 20 μm; n = 5). (C-D, H) Evaluation of P16 expression in discs through tissue immunofluorescence (scale: 20 μm; n = 5). (E-F, I) Evaluation of ADAMTS5 expression in discs through tissue immunofluorescence (scale: 20 μm; n = 5). Data are shown as the mean value (n = 3) ± S.D. Statistical significance is denoted by**p < 0.01, *p < 0.05.

drugs with greater scope and precision, and apply them to relevant diseases.

An in-depth investigation into the mechanisms of drug action is another area where our research is currently lacking. PFD, initially utilized in the treatment of idiopathic pulmonary fibrosis, is a pyridone derivative with broad-spectrum anti-fibrotic properties [59]. It has been shown to possess anti-inflammatory, antioxidative effects, as well as to promote the synthesis of extracellular matrix collagen while inhibiting ECM degradation [60]. Studies suggest that PFD primarily exerts its anti-fibrotic and anti-inflammatory effects by inhibiting pathways such as TGF-β, PDGF and TNF-α [61–63]. Additionally, PFD has been demonstrated to modulate the JAK2/STAT3 signaling pathway and activate the Nrf2 pathway [64,65]. However, research on PFD's role in inhibiting pyroptosis remains sparse, and its underlying mechanisms are yet to be fully explored. Therefore, in our subsequent investigations, we aim to elucidate the specific pathways through which PFD exerts its inhibitory effect on pyroptosis, while also exploring additional related mechanisms and identifying further targeted therapeutic agents.

Furthermore, there is potential for optimization of our materials. The primary function of our PHZ material is drug delivery and sustained release, with pH responsiveness; however, it is somewhat limited in its biological functionality. Recently, there has been increasing interest among researchers in synthesizing nanomaterials with multifunctional properties, nanoparticle-microsphere composites that simultaneously

exhibit anti-inflammatory effects, sustained release, inhibition of ECM degradation, and promotion of collagen synthesis [66]. Additionally, materials that retain their efficacy after degradation, such as bifunctional nanostructured enzymes, which can release substantial amounts of polysulfides upon cellular phagocytosis while also exerting antioxidative effects, have garnered significant attention [67]. Materials with enhanced targeting capabilities are also receiving increased focus, such as metal-phenol nanoparticles that target mitochondria to mitigate oxidative stress [68]. Moving forward, our research will shift toward developing materials with more multifunctional properties and better targeting abilities, while also incorporating drug-carrying capabilities, thereby addressing cell death and disease progression from multiple angles.

5. Conclusion

In this study, we screened the anti-pyroptosis drug PFD in the FDA Medicine Library. Subsequently, we developed PFD@PHZ, a MOF with the functions of lysosomal escape, rapid intracellular drug delivery, and pH-responsive drug controlled release. PFD@PHZ can alleviate IVDD by inhibiting pyroptosis, senescence, and ECM degradation in NPCs. *In vivo* experiments have also shown that PFD@PHZ can effectively alleviate the progression of IVDD in rats, suggesting its considerable potential as a therapeutic option for IVDD treatment.

CRediT authorship contribution statement

Yekai Zhang: Writing – review & editing, Writing – original draft, Methodology, Formal analysis, Data curation. **Jiawei Qiu:** Visualization, Methodology, Formal analysis, Data curation. **Yiji Chen:** Visualization, Methodology, Formal analysis, Data curation, Yu Chen, Visualization, Methodology, Formal analysis, Data curation. **Yu Chen:** Data curation, Project administration, Validation, Writing – review & editing. **Xiaopeng Liu:** Visualization, Validation. **Hanwen Zhang:** Investigation, Data curation. **Hualin Li:** Investigation, Data curation. **Kaiyu Li:** Investigation, Data curation. **Haobo Ye:** Visualization, Supervision. **Yaosen Wu:** Writing – review & editing, Methodology, Conceptualization. **Xiaolei Zhang:** Writing – review & editing, Supervision, Methodology, Conceptualization. **Naifeng Tian:** Writing – review & editing, Supervision, Methodology, Conceptualization.

Declaration of competing interest

The authors declare no competing interests.

Acknowledgements

This study was supported by Zhejiang Provincial Natural Science Foundation of China (LTGY23H060002), National Natural Science Foundation of China (82472501, 82372469).

Appendix A. Supplementary data

Supplementary data to this article can be found online at https://doi.org/10.1016/j.mtbio.2025.101729.

Data availability

Data will be made available on request.

References

[1] D. Hoy, L. March, P. Brooks, F. Blyth, A. Woolf, C. Bain, G. Williams, E. Smith, T. Vos, J. Barendregt, C. Murray, R. Burstein, R. Buchbinder, The global burden of low back pain: estimates from the Global Burden of Disease 2010 study, Ann. Rheum. Dis. 73 (2014) 968–974.

[2] J. Hartvigsen, M.J. Hancock, A. Kongsted, Q. Louw, M.L. Ferreira, S. Genevay, D. Hoy, J. Karppinen, G. Pransky, J. Sieper, R.J. Smeets, M. Underwood, What low back pain is and why we need to pay attention, Lancet (N. Am. Ed.) 391 (2018) 2356–2367.

[3] P.P. Raj, Intervertebral disc: anatomy-physiology-pathophysiology-treatment, Pain Pract. 8 (2008) 18–44.

[4] C.K. Kepler, R.K. Ponnappan, C.A. Tannoury, M.V. Risbud, D.G. Anderson, The molecular basis of intervertebral disc degeneration, Spine J. 13 (2013) 318–330.

[5] F. Yang, W. Liu, Y. Huang, S. Yang, Z. Shao, X. Cai, L. Xiong, Regulated cell death: implications for intervertebral disc degeneration and therapy, J ORTHOP TRANSL 37 (2022) 163–172.

[6] D. Zhou, Y. Mei, C. Song, K. Cheng, W. Cai, D. Guo, S. Gao, J. Lv, T. Liu, Y. Zhou, L. Wang, B. Liu, Z. Liu, Exploration of the mode of death and potential death mechanisms of nucleus pulposus cells, Eur. J. Clin. Invest. 54 (2024) e14226.

[7] K. Sun, C. Yan, X. Dai, Y. Shi, F. Li, L. Chen, J. Sun, Y. Chen, J. Shi, Catalytic nanodots-driven pyroptosis suppression in nucleus pulposus for antioxidant intervention of intervertebral disc degeneration, Adv. Mater. 36 (2024) e2313248.

[8] J. Shi, W. Gao, F. Shao, Pyroptosis: gasdermin-mediated programmed necrotic cell death, Trends Biochem. Sci. 42 (2017) 245–254.

[9] Y. Ge, Y. Chen, C. Guo, H. Luo, F. Fu, W. Ji, C. Wu, H. Ruan, Pyroptosis and intervertebral disc degeneration: Mechanistic insights and therapeutic Implications, J. Inflamm. Res. 15 (2022) 5857–5871.

[10] J.C. Acosta, A. Banito, T. Wuestefeld, A. Georgilis, P. Janich, J.P. Morton, D. Athineos, T. Kang, F. Lasitschka, M. Andrulis, G. Pascual, K.J. Morris, S. Khan, H. Jin, G. Dharmalingam, A.P. Snijders, T. Carroll, D. Capper, C. Pritchard, G. J. Inman, T. Longerich, O.J. Sansom, S.A. Benitah, L. Zender, J. Gil, A complex secretory program orchestrated by the inflammasome controls paracrine senescence, Nat. Cell Biol. 15 (2013) 978–990.

[11] C. Zhou, Q. Guo, J. Lin, M. Wang, Z. Zeng, Y. Li, X. Li, Y. Xiang, Q. Liang, J. Liu, T. Wu, Y. Zeng, S. He, S. Wang, H. Zeng, X. Liang, Single-cell atlas of human ovaries reveals the role of the pyroptotic macrophage in ovarian aging, Adv. Sci. 11 (2024) e2305175.

[12] T. Ohnishi, N. Iwasaki, H. Sudo, Causes of and molecular targets for the treatment of intervertebral disc degeneration: a review, Cells-Basel 11 (2022).

[13] X. Peng, H. Ji, J. Gao, S. Hong, T. Zhang, G. Yang, X. Wu, Y. Gao, K. Wang, YAP1 exacerbates pyroptosis and senescence in nucleus pulposus cells by promoting BNIP3-mediated mitophagy, Int Immunopharmacol 143 (2024) 113434.

[14] C. Li, Y. Zhang, Y. Deng, Y. Chen, C. Wu, X. Zhao, X. Chen, X. Wang, Y. Zhou, X. Zhang, N. Tian, Fisetin suppresses ferroptosis through Nrf2 and attenuates intervertebral disc degeneration in rats, Eur. J. Pharmacol. 964 (2024) 176298.

[15] X. Zhao, S. Su, C. Wu, Y. Deng, Y. Chen, T. Yu, C. Li, Y. Zhang, X. Wang, Y. Zhou, X. Zhang, High-throughput screening-based design of multifunctional natural polyphenol nano-vesicles to accelerate diabetic wound healing, J. Nanobiotechnol. 22 (2024) 725.

[16] J.J. Hu, X. Liu, S. Xia, Z. Zhang, Y. Zhang, J. Zhao, J. Ruan, X. Luo, X. Lou, Y. Bai, J. Wang, L.R. Hollingsworth, V.G. Magupalli, L. Zhao, H.R. Luo, J. Kim, J. Lieberman, H. Wu, FDA-approved disulfiram inhibits pyroptosis by blocking gasdermin D pore formation, Nat. Immunol. 21 (2020) 736–745.

[17] Y. Chen, X. Cao, B. Pan, H. Du, B. Li, X. Yang, X. Chen, X. Wang, T. Zhou, A. Qin, C. Zhao, J. Zhao, Verapamil attenuates intervertebral disc degeneration by suppressing ROS overproduction and pyroptosis via targeting the Nrf2/TXNIP/NLRP3 axis in four-week puncture-induced rat models both in vivo and in vitro, Int Immunopharmacol 123 (2023) 110789.

[18] W. Chen, Z. Deng, J. Zhu, L. Yuan, S. Li, Y. Zhang, J. Wu, Z. Huang, T. Qin, W. Ye, Rosuvastatin suppresses TNF-alpha-induced matrix catabolism, pyroptosis and senescence via the HMGB1/NF-kappaB signaling pathway in nucleus pulposus cells, ACTA BIOCH BIOPH SIN 55 (2023) 795–808.

[19] P. Li, F. Xiong, H. Xing, S. Hu, N. Zhang, Retinoic acid inhibits the pyroptosis of degenerated nucleus pulposus cells by activating Sirt1-SOD2 signaling, Connect. Tissue Res. 64 (2023) 337–349.

[20] X. Wang, F. Wu, Y. Huang, H. Li, X. Cao, Y. You, Z. Meng, K. Sun, X. Shen, Matrine suppresses NLRP3 inflammasome activation via regulating PTPN2/JNK/SREBP2 pathway in sepsis, Phytomedicine 109 (2023) 154574.

[21] G. Tezcan, E.E. Garanina, M. Alsaadi, Z.E. Gilazieva, E.V. Martinova, M. I. Markelova, S.S. Arkhipova, S. Hamza, A. McIntyre, A.A. Rizvanov, S. F. Khaiboullina, Therapeutic potential of pharmacological targeting NLRP3 inflammasome complex in cancer, Front. Immunol. 11 (2020) 607881.

[22] G. Jing, J. Zuo, Q. Fang, M. Yuan, Y. Xia, Q. Jin, Y. Liu, Y. Wang, Z. Zhang, W. Liu, X. Wu, X. Song, Erbin protects against sepsis-associated encephalopathy by attenuating microglia pyroptosis via IRE1alpha/Xbp1s-Ca(2+) axis, J Neuroinflamm 19 (2022) 237.

[23] M. Ghazipura, M.J. Mammen, B.D. Bissell, M. Macrea, D.D. Herman, S.M. Hon, F. Kheir, Y.H. Khor, S.L. Knight, G. Raghu, K.C. Wilson, T. Hossain, Pirfenidone in progressive pulmonary fibrosis: a systematic review and meta-analysis, ANN AM THORAC SOC 19 (2022) 1030–1039.

[24] Y. Liang, Y. Yan, N. Liu, J. Wang, C. Fang, Shengxian decoction improves lung function in rats with bleomycin-induced idiopathic pulmonary fibrosis through the inhibition of PANoptosis, J. Ethnopharmacol. 329 (2024) 118153.

[25] F. Chen, N. Duan, X. Zhang, W. Zhang, [Effect of Fuzheng Tongluo Granules on macrophage pyroptosis in rat model with pulmonary fibrosis based on NLRP3/caspase-1/GSDMD pathway], Zhongguo Zhongyao Zazhi 49 (2024) 6399–6406.

[26] S.B.G. Blanquer, D.W. Grijpma, A.A. Poot, Delivery systems for the treatment of degenerated intervertebral discs, Adv. Drug Deliv. Rev. 84 (2015) 172–187.

[27] I.L. Mohd Isa, S.A. Mokhtar, S.A. Abbah, M.B. Fauzi, A. Devitt, A. Pandit, Intervertebral disc degeneration: biomaterials and tissue engineering strategies toward precision medicine, Adv Healthc Mater 11 (2022) e2102530.

[28] R.D. Bowles, L.A. Setton, Biomaterials for intervertebral disc regeneration and repair, Biomaterials 129 (2017) 54–67.
[29] F. Colella, J.P. Garcia, M. Sorbona, A. Lolli, B. Antunes, D. D'Atri, F.P.Y. Barre, J. Oieni, M.L. Vainieri, L. Zerrillo, S. Capar, S. Hackel, Y. Cai, L.B. Creemers, Drug delivery in intervertebral disc degeneration and osteoarthritis: selecting the optimal platform for the delivery of disease-modifying agents, J Control Release 328 (2020) 985–999.
[30] W. Liu, Z. Ma, Y. Wang, J. Yang, Multiple nano-drug delivery systems for intervertebral disc degeneration: current status and future perspectives, Bioact. Mater. 23 (2023) 274–299.
[31] L. Frapin, J. Clouet, V. Delplace, M. Fusellier, J. Guicheux, C. Le Visage, Lessons learned from intervertebral disc pathophysiology to guide rational design of sequential delivery systems for therapeutic biological factors, Adv. Drug Deliv. Rev. 149–150 (2019) 49–71.
[32] S. Ravindran, J.K. Suthar, R. Rokade, P. Deshpande, P. Singh, A. Pratinidhi, R. Khambadkhar, S. Utekar, Pharmacokinetics, metabolism, distribution and permeability of nanomedicine, Curr Drug Metab 19 (2018) 327–334.
[33] S. Hossen, M.K. Hossain, M.K. Basher, M.N.H. Mia, M.T. Rahman, M.J. Uddin, Smart nanocarrier-based drug delivery systems for cancer therapy and toxicity studies: a review, J. Adv. Res. 15 (2019) 1–18.
[34] H. Zhou, J. He, R. Liu, J. Cheng, Y. Yuan, W. Mao, J. Zhou, H. He, Q. Liu, W. Tan, C. Shuai, Y. Deng, Microenvironment-responsive metal-phenolic network release platform with ROS scavenging, anti-pyroptosis, and ECM regeneration for intervertebral disc degeneration, Bioact. Mater. 37 (2024) 51–71.
[35] S. Wei, S. Zhou, W. Huang, X. Zan, W. Geng, Efficient delivery of antibodies intracellularly by Co-assembly with hexahistidine-metal assemblies (HmA), Int. J. Nanomed. 16 (2021) 7449–7461.
[36] M. Wu, Y. Yang, Metal-organic framework (MOF)-Based drug/cargo delivery and cancer therapy, Adv. Mater. 29 (2017).
[37] J. Yang, Y. Yang, Metal-organic frameworks for biomedical applications, Small 16 (2020) e1906846.
[38] B. Diamant, J. Karlsson, A. Nachemson, Correlation between lactate levels and pH in discs of patients with lumbar rhizopathies, Experientia 24 (1968) 1195–1196.
[39] T. Kitano, J.E. Zerwekh, Y. Usui, M.L. Edwards, P.L. Flicker, V. Mooney, Biochemical changes associated with the symptomatic human intervertebral disk, CLIN ORTHOP RELAT R (1993) 372–377.
[40] K. Masuda, Y. Aota, C. Muehleman, Y. Imai, M. Okuma, E.J. Thonar, G. B. Andersson, H.S. An, A novel rabbit model of mild, reproducible disc degeneration by an anulus needle puncture: correlation between the degree of disc injury and radiological and histological appearances of disc degeneration, Spine 30 (2005) 5–14.
[41] Y. Li, H. Li, S. Liu, P. Pan, X. Su, H. Tan, D. Wu, L. Zhang, C. Song, M. Dai, Q. Li, Z. Mao, Y. Long, Y. Hu, C. Hu, Pirfenidone ameliorates lipopolysaccharide-induced pulmonary inflammation and fibrosis by blocking NLRP3 inflammasome activation, Mol. Immunol. 99 (2018) 134–144.
[42] D. Samartzis, A. Borthakur, I. Belfer, C. Bow, J.C. Lotz, H. Wang, K.M.C. Cheung, E. Carragee, J. Karppinen, Novel diagnostic and prognostic methods for disc degeneration and low back pain, Spine J. 15 (2015) 1919–1932.
[43] P.A. Vergroesen, I. Kingma, K.S. Emanuel, R.J.W. Hoogendoorn, T.J. Welting, B. J. van Royen, J.H. van Dieen, T.H. Smit, Mechanics and biology in intervertebral disc degeneration: a vicious circle, OSTEOARTHR CARTILAGE 23 (2015) 1057–1070.
[44] I.L. Mohd Isa, S.L. Teoh, N.H. Mohd Nor, S.A. Mokhtar, Discogenic low back pain: anatomy, pathophysiology and treatments of intervertebral disc degeneration, Int. J. Mol. Sci. 24 (2022).
[45] P. Wen, B. Zheng, B. Zhang, T. Ma, L. Hao, Y. Zhang, The role of ageing and oxidative stress in intervertebral disc degeneration, Front. Mol. Biosci. 9 (2022) 1052878.
[46] K. Newton, A. Strasser, N. Kayagaki, V.M. Dixit, Cell death, Cell 187 (2024) 235–256.
[47] P. Yu, X. Zhang, N. Liu, L. Tang, C. Peng, X. Chen, Pyroptosis: mechanisms and diseases, Signal Transduct Tar 6 (2021) 128.
[48] D. Bertheloot, E. Latz, B.S. Franklin, Necroptosis, pyroptosis and apoptosis: an intricate game of cell death, Cell Mol Immunol 18 (2021) 1106–1121.
[49] J. Luo, Y. Yang, X. Wang, X. Chang, S. Fu, Role of pyroptosis in intervertebral disc degeneration and its therapeutic implications, Biomolecules 12 (2022).
[50] A. Kamali, R. Ziadlou, G. Lang, J. Pfannkuche, S. Cui, Z. Li, R.G. Richards, M. Alini, S. Grad, Small molecule-based treatment approaches for intervertebral disc degeneration: current options and future directions, Theranostics 11 (2021) 27–47.
[51] S. Hirano, A. Higashimori, Y. Nagami, Y. Nadatani, T. Tanigawa, M. Ominami, S. Fukunaga, K. Otani, S. Hosomi, F. Tanaka, N. Kamata, K. Taira, T. Watanabe, Y. Fujiwara, Pirfenidone prevents esophageal stricture by inhibiting nucleotide binding oligomerization domain like receptor protein 3 inflammasome activation, J Gastroen Hepatol 37 (2022) 1096–1106.
[52] W. Shao, J. Zhang, Z. Yao, P. Zhao, B. Li, W. Tang, J. Zhang, Cannabidiol suppresses silica-induced pulmonary inflammation and fibrosis through regulating NLRP3/TGF-beta1/Smad2/3 pathway, Int Immunopharmacol 142 (2024) 113088.
[53] S. Razaq, J.P. Urban, R.J. Wilkins, Regulation of intracellular pH by bovine intervertebral disc cells, Cell. Physiol. Biochem. 10 (2000) 109–115.
[54] S. Razaq, R.J. Wilkins, J.P.G. Urban, The effect of extracellular pH on matrix turnover by cells of the bovine nucleus pulposus, Eur. Spine J. 12 (2003) 341–349.
[55] S. Forli, R. Huey, M.E. Pique, M.F. Sanner, D.S. Goodsell, A.J. Olson, Computational protein-ligand docking and virtual drug screening with the AutoDock suite, Nat. Protoc. 11 (2016) 905–919.
[56] J. Yan, Y. Zhang, H. Yu, Y. Zong, D. Wang, J. Zheng, L. Jin, X. Yu, C. Liu, Y. Zhang, F. Jiang, R. Zhang, X. Fang, T. Xu, M. Li, J. Di, Y. Lu, X. Ma, J. Zhang, W. Jia, C. Hu, GPSM1 impairs metabolic homeostasis by controlling a pro-inflammatory pathway in macrophages, Nat. Commun. 13 (2022) 7260.
[57] D. Wang, Z. Pang, H. Yu, B. Thiombiano, A. Walmsley, S. Yu, Y. Zhang, T. Wei, L. Liang, J. Wang, X. Wen, H.J. Bouwmeester, R. Yao, Z. Xi, Probing strigolactone perception mechanisms with rationally designed small-molecule agonists stimulating germination of root parasitic weeds, Nat. Commun. 13 (2022) 3987.
[58] X. Zhou, Y. Yang, S. Wang, X. Liu, Surface Plasmon resonance microscopy: From single-molecule sensing to single-cell imaging, Angew Chem int Edit 59 (2020) 1776–1785.
[59] P.W. Noble, C. Albera, W.Z. Bradford, U. Costabel, M.K. Glassberg, D. Kardatzke, T. E.J. King, L. Lancaster, S.A. Sahn, J. Szwarcberg, D. Valeyre, R.M. du Bois, Pirfenidone in patients with idiopathic pulmonary fibrosis (CAPACITY): two randomised trials, Lancet (N. Am. Ed.) 377 (2011) 1760–1769.
[60] Z. Cao, Y. Liu, Z. Zhang, P. Yang, Z. Li, M. Song, X. Qi, Z. Han, J. Pang, B. Li, X. Zhang, H. Dai, J. Wang, C. Wang, Pirfenidone ameliorates silica-induced lung inflammation and fibrosis in mice by inhibiting the secretion of interleukin-17A, Acta Pharmacol. Sin. 43 (2022) 908–918.
[61] Q. Lv, J. Wang, C. Xu, X. Huang, Z. Ruan, Y. Dai, Pirfenidone alleviates pulmonary fibrosis in vitro and in vivo through regulating Wnt/GSK-3beta/beta-catenin and TGF-beta1/Smad2/3 signaling pathways, Mol. Med. 26 (49) (2020).
[62] R. Iswandana, B.T. Pham, S. Suriguga, T. Luangmonkong, L.A. van Wijk, Y.J. M. Jansen, D. Oosterhuis, H.A.M. Mutsaers, P. Olinga, Murine precision-cut intestinal slices as a potential screening tool for antifibrotic drugs, Inflamm. Bowel Dis. 26 (2020) 678–686.
[63] W.H. Abdulaal, U.M. Omar, M. Zeyadi, D.S. El-Agamy, N.A. Alhakamy, S.R. M. Ibrahim, N.A.R. Almalki, H.Z. Asfour, M.W. Al-Rabia, G.A. Mohamed, M. Elshal, Pirfenidone ameliorates ANIT-induced cholestatic liver injury via modulation of FXR, NF-small ka, CyrillicB/TNF-alpha, and Wnt/GSK-3beta/beta-catenin signaling pathways, Toxicol Appl Pharm 490 (2024) 117038.
[64] R. Xie, S. Chen, F. Li, L. Yang, B. Yu, Pirfenidone attenuates nonalcoholic fatty liver disease through activation of the nuclear factor erythroid 2-related factor 2 (Nrf2) signaling pathway, J Biochem Mol Toxic 37 (2023) e23251.
[65] Q. Tang, C. Xing, M. Li, Q. Jia, C. Bo, Z. Zhang, Pirfenidone ameliorates pulmonary inflammation and fibrosis in a rat silicosis model by inhibiting macrophage polarization and JAK2/STAT3 signaling pathways, Ecotox Environ Safe 244 (2022) 114066.
[66] L. Zhou, F. Cai, H. Zhu, Y. Xu, J. Tang, W. Wang, Z. Li, J. Wu, Z. Ding, K. Xi, L. Chen, Y. Gu, Immune-defensive microspheres promote regeneration of the nucleus pulposus by targeted entrapment of the inflammatory cascade during intervertebral disc degeneration, Bioact. Mater. 37 (2024) 132–152.
[67] Y. Shi, H. Li, D. Chu, W. Lin, X. Wang, Y. Wu, K. Li, H. Wang, D. Li, Z. Xu, L. Gao, B. Li, H. Chen, Rescuing nucleus pulposus cells from senescence via dual-functional greigite nanozyme to alleviate intervertebral disc degeneration, Adv. Sci. 10 (2023) e2300988.
[68] Q. Chen, Q. Qian, H. Xu, H. Zhou, L. Chen, N. Shao, K. Zhang, T. Chen, H. Tian, Z. Zhang, M. Jones, K.Y.H. Kwan, M. Sewell, S. Shen, X. Wang, M.A. Khan, P. Makvandi, S. Jin, Y. Zhou, A. Wu, Mitochondrial-targeted metal-phenolic nanoparticles to attenuate intervertebral disc degeneration: alleviating oxidative stress and mitochondrial dysfunction, ACS Nano 18 (2024) 8885–8905.